JMEPEG (2009) 18:563–568
DOI: 10.1007/s11665-009-9363-4

1059-9495/$19.00

Fatigue Performance of Nitinol Round Wire with Varying Cold Work Reductions

Jeremy E. Schaffer and David L. Plumley

(Submitted October 8, 2008; in revised form November 13, 2008)

The role of cold work reduction and its effect on fatigue properties are examined by means of rotary beam fatigue testing. In this study, processing parameters from the initial ingot to the final size before finish drawing were held constant. Fatigue specimens were prepared with between 20 and 55% cold work in five percent increments. These samples were subsequently heat treated, cut into test sections at room temperature, and subjected to strain-controlled fatigue testing in a temperature-controlled RO water bath at a constant 10 °C above the measured active austenitic finish temperature (A_f). An empirical analysis of the relationship between final reduction prior to heat treatment and fatigue lifetime is presented. Under alternating strain amplitudes greater than 1%, the 20 to 30% cold work level was found to deliver the greatest mean cycles to failure. Supplemental to the fatigue data, mechanocyclic and thermomechanical data are also presented as they evolve with prior retained cold work.

Keywords nitinol wire, nitinol processing, nitinol cold work, strain fatigue

1. Introduction

There are many processing parameters which can influence the mechanical, thermal, and bioreactive properties of nitinol wire and its suitability for particular applications (Ref 1-3). Variables may include: ingot composition; inclusion particle size and shape distribution; cold work history; annealing temperature, stress, atmosphere and resultant microstructural cell size; surface conditioning including oxide thickness, acidic oxide removal or mechanical polishing; shape-setting temperature and others. Use of nitinol as an implantable material requires an understanding of specific structure-property relationships. For long term implants, life expectancy before fracture under cyclic loading should be predictable given a set of processing and service conditions. Studies correlating material processing to fatigue behavior are therefore important in robust device design.

Significant research has been dedicated to understanding how Nitinol behaves in the body from the viewpoint of a biological host response (Ref 4-6); much less literature has been published which quantitatively correlates structure with mechanical properties. It could be because chemical studies are generally easier to carry out and interpret than the sometimes confounding mechanical response of Nitinol. Perhaps for this reason, there is an even greater dearth of information in the area of fine wire for medical devices such as guidewires, braided vascular stents, embolic filters, and other Nitinol wire-based devices. Biomedical engineers need to understand not only how such variables affect reversible inelastic behavior, but also be able to quantify their effect on fatigue life. Up to the time of this writing, with few exceptions (Ref 7-10), little work had been published on the fatigue behavior of fine Nitinol wires as a function of wire processing variables.

Plastic deformation through cold wire drawing of most metallic alloys results in increased mechanical strength that is attributable to an increase in lattice defects, many of which are dislocations. It is largely the strain fields associated with these dislocations that result in implant durability and strength or in some cases can lead to brittleness and failure. In the case of Nitinol, cold work and the associated dislocation network density can dramatically influence mechanical properties (Ref 1, 3). In this investigation, the goal was to elucidate the effect of cold work on mechanocyclic, mechanothermal, and thermocyclic properties. To accomplish this, nominally Ti-50.9 at.% Ni binary NiTi wires having an ingot A_s temperature of −17 °C were produced with variable retained cold work prior to heat treatment. In order to mimic field use, the nominally 50-nm thick process-intrinsic oxide barrier was left intact throughout testing.

2. Experimental

The initial material for the experiment was 6.35 mm diameter wire of Ti-50.8 at.% Ni which was repeatedly drawn and annealed to staged diameters in preparation for final full annealing. Interpass and final annealing processes were performed at a temperature of 650-850 °C at a sufficient dwell time to ensure complete recrystallization. Wires were conventionally wet-drawn using natural diamond drawing dies and

This article is an invited paper selected from presentations at Shape Memory and Superelastic Technologies 2008, held September 21-25, 2008, in Stressa, Italy, and has been expanded from the original presentation.

Jeremy E. Schaffer and **David L. Plumley**, Fort Wayne Metals Research Products Corporation, 9609 Ardmore Avenue, Fort Wayne, IN 46809. Contact e-mail: jeremy_schaffer@fwmetals.com, dave_plumley@fwmetals.com.

oil-based lubricants to a finished diameter of 0.32 mm. All of the wires were heat treated at 490 °C for a dwell time of 15 min in an air-stirred fluidized bed with alumina media and quenched in ambient air at nominally 25 °C. In order to reduce the effects of ingot compositional variability, the total quantity of material consumed was limited; total sample material comprised approximately 2 kg from a consecutive billet location.

After the 490 °C heat treatment, active sample transformation temperatures were analyzed using bend and free recovery (BFR) methodology using a proprietary digital video analysis apparatus per standard ASTM F2082-06 (Ref 11). Cyclic and monotonic uniaxial tensile properties were measured at 37 °C using an Instron Model 5565 Tensile Test Bench equipped with an environmental chamber. Near-surface microstructure and oxide thickness determination was performed using a combination of focused ion beam (FIB) milling and transmission electron microscopy (TEM). Fatigue behavior was characterized using rotary beam fatigue test equipment manufactured by Positool, Inc. at 3600 rpm in a temperature-controlled, continuously flowing water bath. Ten specimens from each cold work condition were tested at alternating strain amplitudes ranging from 0.9 to 2.5% to a maximum of 1×10^8 cycles.

Fatigue sample geometry was calculated based on the assumption of elastic loading with a central neutral axis using Eq 1. While this approach was used as a convention, the calculated strain amplitude and strain ratio are likely not a perfect representation of the true material state. Nitinol is known to exhibit a stress-strain response that is asymmetric in tensile versus compressive loading (Ref 1, 14). During initial cycling where compression requires greater strain to begin transformation, we expect a dynamic neutral axis shift away from the tensile surface. This behavior would alter the strain ratio and thus the effective crack opening strain range and may be an important and dynamic variable in bend-type testing of nitinol wire.

$$\varepsilon_a = d/2R \qquad \text{(Eq 1)}$$

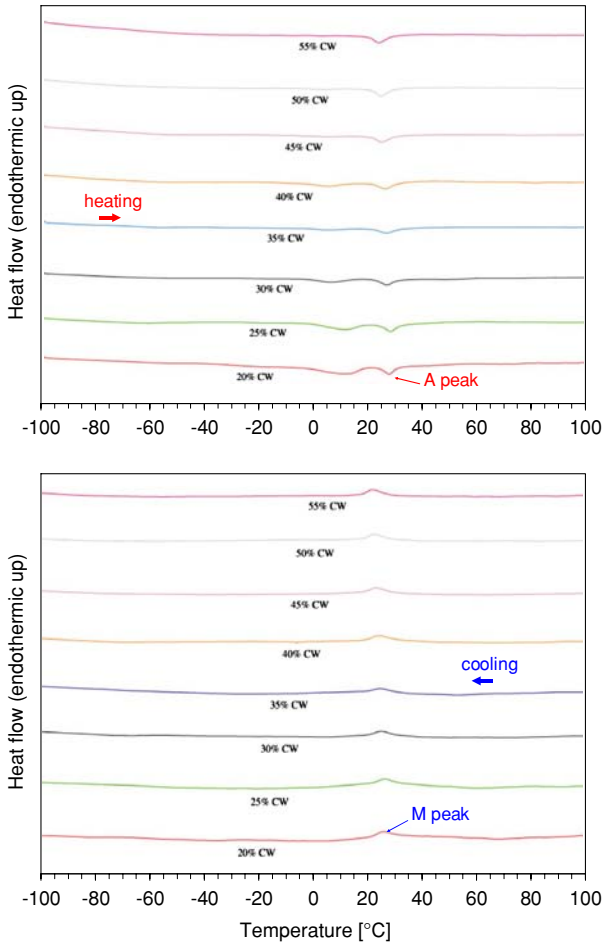

Fig. 1 DSC curves of heat-treated nitinol wires. Material was scanned in the active state over the range of −100 to 100 °C

3. Results and Discussion

3.1 DSC Analysis

Differential scanning calorimetry (DSC) was used to examine thermal phase transformation points in both the fully annealed as well as active heat-treated states. The martensitic and austenitic transformation ranges were found to be consistent to be within 10 °C for all the specimens tested, showing a small downward shift with increasing cold work similar to other work. Multistep transformations were evident in the heating curves for samples that were cold worked between 20 and 40%. The resultant transformations shown in Fig. 1 were described by the two-step transformation as: martensite (M) → R′ and R′ → B2 (Ref 12). Multiple peaks were not visually evident in the cooling direction or in the heating direction above ~40% cold work indicating likely the thermal superposition or single stage transformation (Ref 13).

3.2 BFR Analysis

All investigated samples were taken consecutively from a single nitinol parent ingot and were found to possess similar austenitic transformation temperatures. Bend and free recovery testing (BFR) was used in order to characterize the active or process-dependent, transformation temperature range. At 0.32 mm in the heat treated state, the austenitic start and finish temperatures (A_s and A_f) were derived from computer-generated plots that were collected using digital video analysis.

The BFR curve shown in Fig. 2 clearly exhibits at least three distinct regions: a martensitic flat line at the left, initial recovery to −10 °C, essentially rate constant recovery until 20.5 °C (A_s), and an increasing rate toward completion through the austenitic transformation. The actual three regions of recovery may comprise: complex transition from B19′ to an energetically preferred R-phase variant back to B19′ before transitioning to B2 austenite. Duerig described possible stress-induced *R* transformation at low temperatures in (Ref 14). Here, strain is initially imparted at 218 K, below M_f and within the range described by Duerig. Thus a mixed strain-stabilized *R*-phase, B19′ starting point is possible. The strain stabilization of *R*-phase in this temperature range may also explain the lack of a deconvoluted *R*-peak in the DSC results: subtract the strain imparted for BFR, and eliminate the *R*-phase. Verification of this phenomenon should be explored further via in situ TEM deformation studies.

3.3 Tensile Properties

The as-drawn material showed a large increase in both the engineering yield and ultimate strength as a function of cold work as exemplified in Fig. 3. Cold work was also accompanied by a large reduction in strain to rupture, similar to other published studies (Ref 1, 15). The modulus of elasticity was also found to increase in the as-worked material from a minimum at 30% cold work of 40 GPa to a maximum at 55% cold work of about 60 GPa. The fluctuation in elastic modulus has been reported in other studies and is ascribed to initial martensite reorientation and variant activity in the fully developing martensitic structure (Ref 16) (see Fig. 3 inset).

In the heat-treated condition, samples were cyclically and monotonically tensile tested at 37 °C. A positive correlation was found between ultimate strength, loading plateau strength, and stress hysteresis relative to prior retained cold work. No clear relationship was found between the permanent set after a 6% strain departure and the prior cold work (see Fig. 4 and 5).

3.4 Fatigue Properties

Ten specimens were cycled to failure from each condition using a rotary beam fatigue apparatus until failure or until a maximum of 10^8 cycles. The testing was carried out in reverse osmosis (RO)-purified water that was continuously flowing and controlled at a temperature of 37 ± 2 °C. A strain-life representation of the data is depicted in Fig. 6. At alternating strain levels above 1%, the samples in the 20 to 35% cold work range consistently lasted longer than the samples with greater than 40% cold work. The downward shift in life with cold work is readily evident in the normalized life plot shown in Fig. 7. A mixture of high cycle runouts and fractures was observed for all samples tested at the 0.90% alternating strain level.

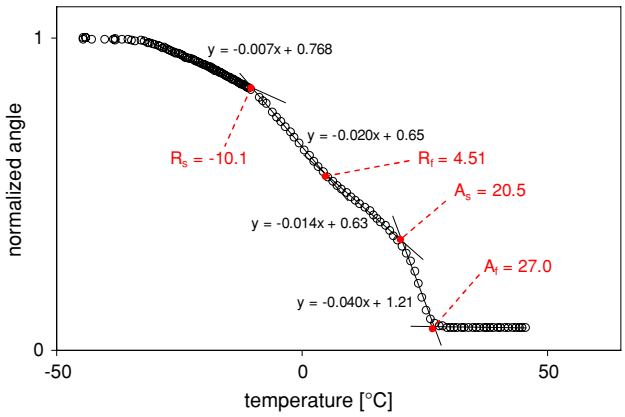

Fig. 2 Bend and free recovery curve as per ASTM F2082 for sample at 45% cold work. Note apparent multi-stage transformation as strained sample is recovered. Ordinate angle axis has been normalized to maximum bend angle (A/A_{max})

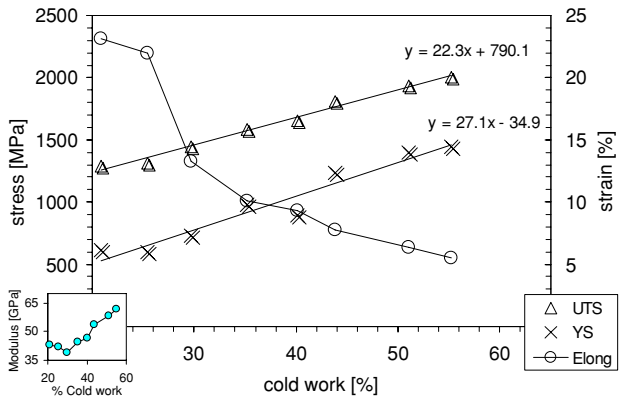

Fig. 3 Uniaxial tensile property data for eight cold work levels in the as-drawn condition where UTS is ultimate tensile strength, YS is 0.2% yield strength, and Elong is the strain to rupture

3.5 Scanning Electron Microscopy

Scanning electron microscopy (SEM) was used to characterize the fatigue crack-initiating features by location, type and

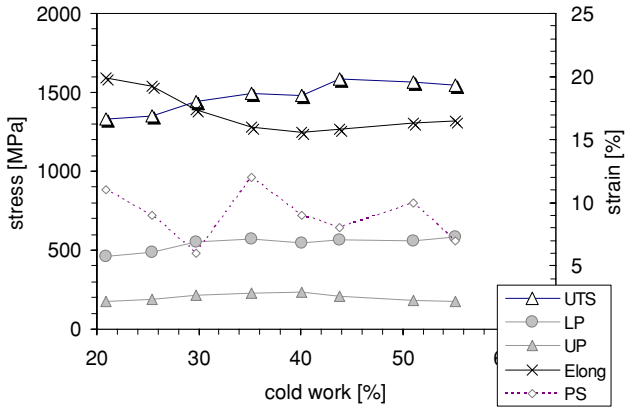

Fig. 4 Cyclic tensile property data for eight cold work levels after heat treatment, where LP is the loading, stress-induced B19′, plateau stress; UP is the unloading plateau stress; and PS is 100× permanent set after a single 6% superelastic cycle

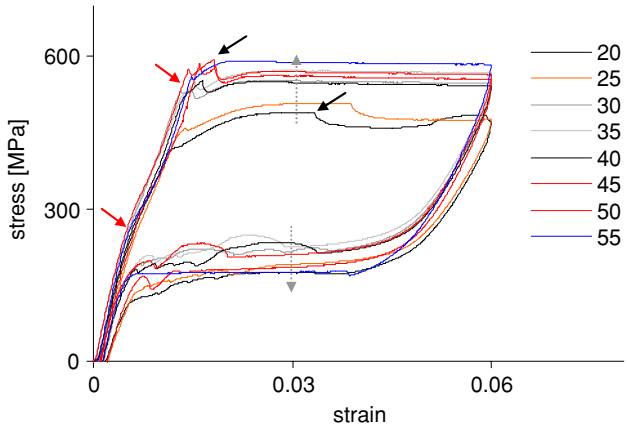

Fig. 5 Six percent strain cycle at 37 °C, 10^{-3} s^{-1} strain rate for all the samples. Gray vertical arrows show general plateau trends with increasing cold work. Black diagonal arrows indicate evidence of possible diffuse yield drop associated with the onset of martensite plate variants propagating into a mixed elastically strained austenite/*R*-phase matrix or the possible onset of detwinning of major B19′ variants (Ref 18). Red arrows show the onset of elastic deviation possibly due to microtwinning or the presence of a stress-induced *R*-phase plateau running from 0.6 to about 1.3%

geometry. Fracture analysis was only performed for fractures that occurred at the 0.9% strain level. Under this condition, two types of initiating features were found: melt-intrinsic inclusions and melt-extrinsic oxide defects. Representative initiating defects are shown in Fig. 8. A summary of defect counts versus cold work is shown in Fig. 9.

Prior studies completed for other medically relevant alloys have shown the importance of melt-intrinsic constituent particle distributions on total fatigue life, both in terms of defect size and proximity to the free wire surface (Ref 17). Crack-initiating defect states were measured here in a similar manner and compared with total life. The resultant data, plotted in Fig. 10,

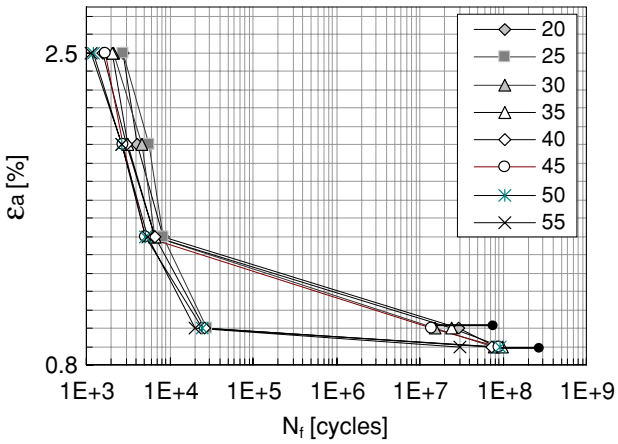

Fig. 6 Strain-controlled fatigue cycles to failure plotted on the abscissa as a function of ordinate alternating strain (ε_a). Lines terminating in a solid-filled circle represent an averaged mix of runouts and fractures

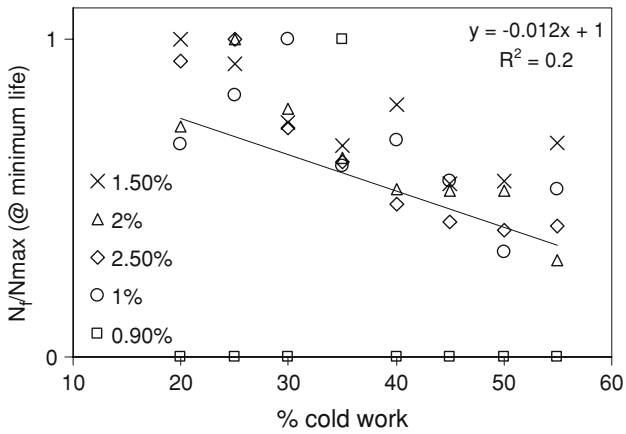

Fig. 7 This chart represents the following operations: (1) minimum cycles to fracture data were grouped for each cold work level, (2) the maximum cycle life value was taken at each strain level, and (3) data was normalized at each strain level by dividing into this maximum. The upper left "X" on the plot indicates that the 20% cold work level gave the greatest number of minimum cycles to failure (10 percentile) at the 1.5% strain level

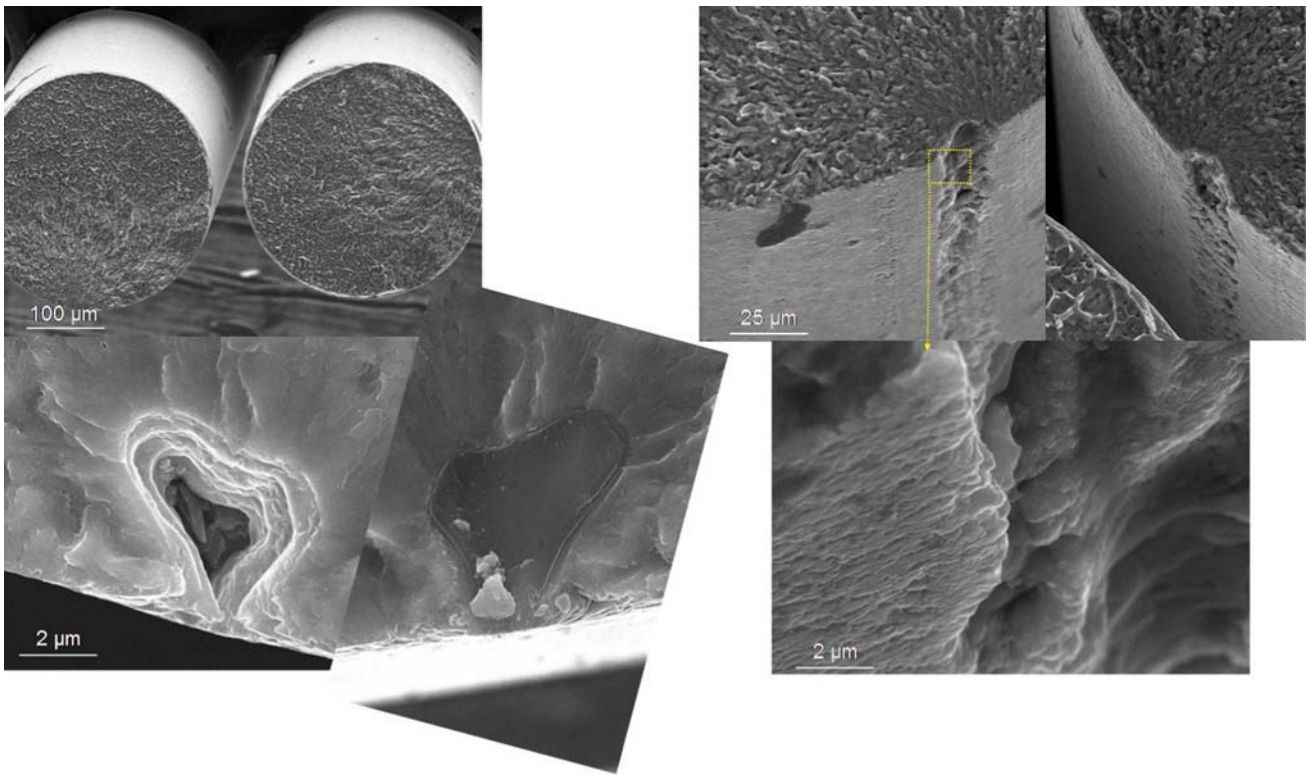

Fig. 8 Scanning electron microscopy (SEM) image collages showing (left) failure at a melt intrinsic 5.5-µm TiC inclusion in a 40% cold work sample ran at 0.9% alternating strain to 24,120 cycles and (right) failure an melt-extrinsic, 6-µm deep oxide defect in a 55% cold work sample tested to failure at 0.9% alternating strain in 32,976 cycles

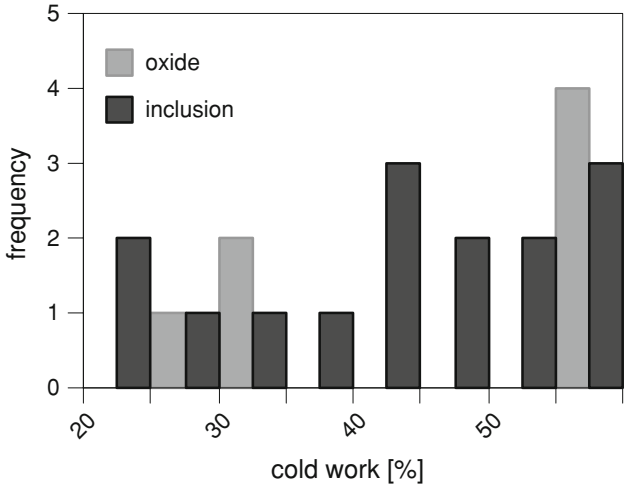

Fig. 9 Crack-initiating features collected from samples that fractured at 0.9% alternating strain. Types: oxide refers to extrinsic oxide surface defects similar to depiction in Fig. 8, right; inclusion refers to melt-intrinsic, primarily titanium carbide (TiC), constituent particles

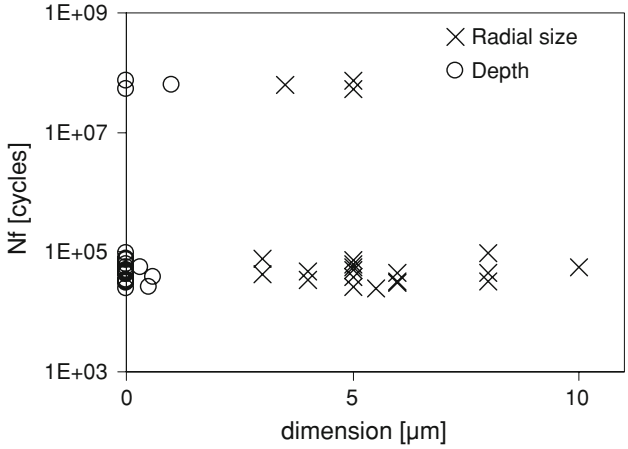

Fig. 10 Plot showing ordinate cycles to failure compared to abscissa radial inclusion size and depth from the surface normal stress-free interface (wire surface)

does not show a definable trend. While contributing factors to this lack of correlation will not be made explicit within this manuscript, possible explanation for this phenomenon could be related to the relatively insignificant contribution of crack propagation to total fatigue life (Ref 17).

4. Conclusions

A multistage transformation was observed in BFR testing that was not seen as separate *R*-phase transformation peaks in the DSC data. It is postulated that this may have proceeded by low temperature strain-stabilization as: (1) matrix cooled to 218 K resulting in B19′ matrix, (2) strain accommodation in B19′ resulted in some energetically favorable *R*-phase stabilization, (3) free recovery during heating yielded separate recovery via distinct routes: *R*-phase → B2 and B19′ → B2 thus resulting in the observed multistage BFR character. Further in situ TEM analysis is needed to develop a full mechanistic explanation of this phenomenon.

Tensile testing of the heat-treated samples at +10 °C relative to the measured A_f and a strain rate of 10^{-3} s^{-1} showed a yield drop within the first 1 to 3% strain. Without further in situ TEM structural data, it is inconclusive whether this load drop was associated with inhomogeneous strain-stabilization and reorientation of B19′ variants, the onset of detwinning in some B19′ variants, or other mechanisms. A deviation from elastic B2 loading, possibly related to stress-induced *R*-phase transformation plateaus, was evident as departure from otherwise linear loading within the first 0.6 to 1.3% strain of all the heat-treated samples.

Fatigue life was maximized in the range of 20 to 35% retained cold work as measured at strain levels exceeding about 1%. Bimodal failure conditions were found for all the samples at the 0.9% alternating strain level where this conundrum was observed: for all cold work levels most samples ran to the 10^8 cycle limit (5/10 to 9/10) while all the levels also showed low level fractures (2.1×10^4 to 5.4×10^7 cycles) at a mixture of melt-intrinsic constituent particles and extrinsic surface oxide defects.

A bimodal lifetime distribution comprising fatigue lifetimes on the order of 10^4 cycles mixed with lifetimes greater than 10^8 cycles was observed at alternating strain amplitudes of 0.9%. One possible explanation for this phenomenon is related to defect seeding associated with the initial defect state (IDS). The IDS includes the statistical distribution of inclusions, surface defects, grain boundaries, etc., and may seed nitinol for bimodal failure lifetime distributions as follows. In essence, if a defect is seeded in the critical fatigue strain zone that initiates small crack regime growth, the short lifetime may not vary much by initial defect size because of rapid crack advancement of the seeded failure after a relatively constant incubation period. In critically loaded sections where such defect seeding is not present, effective loading may yield fatigue lifetimes that are orders of magnitude greater. Some level of protection may also be induced near larger defects due to proximal crack-tip B19′, which has been shown to possess lower crack growth susceptibility relative to the B2 phase (Ref 19). This protective crack tip phase transformation mechanism would not be present in most other alloys. These mechanisms are actively being investigated further in continuation of this study with unlimited runout cycle criteria.

References

1. K. Gall, J. Tyber, V. Brice, C.P. Frick, H.J. Maier, and N. Morgan, Tensile Deformations of NiTi Wires, *J. Biomed. Mater. Res.*, 2005, **75A**, p 810–823
2. S.W. Robertson, X.Y. Gong, and R.O. Ritchie, Effect of Product Form and Heat Treatment on the Crystallographic Texture of Austenitic Nitinol, *J. Mater. Sci.*, 2006, **41**, p 621–630
3. M.H. Wu, Effects of Phase Transformations on Fatigue Endurance of a Superelastic NiTi Alloy, *J. ASTM Int.*, 2007, **4**(3), p 1–6
4. E. McLucas, Y. Rochev, and W.M. Carroll, Analysis of the Effects of Surface Treatments on Nickel Release from Nitinol Wires and Their Impact on Candidate Gene Expression in Endothelial Cells, *J. Mater. Sci. Mater. Med.*, 2008, **19**, p 975–980
5. M. Assad, L.H. Yahia, C.H. Rivard, and N. Lemieux, In Vitro Biocompatibility Assessment of a Nickel-Titanium Alloy Using Electron Microscopy In Situ End-Labeling (EM-ISEL), *J. Biomed. Mater. Res.*, 1998, **41A**, p 154–161

6. J.C. Wataha, P.E. Lockwood, M. Marek, and M. Ghazi, Ability of Ni-Containing Biomedical Alloys to Activate Monocytes and Endothelial Cells In Vitro, *J. Biomed. Mater. Res.*, 1999, **45A**, p 251–257
7. M.M. Patel, Characterizing Fatigue Response of Nickel-Titanium Alloys by Rotary Beam Testing, *J. ASTM Int.*, 2007, **4**, p 1–11
8. M. Reinoehl, D. Bradley, R. Bouthot, and J. Proft, The Influence of Melt Practice on Final Fatigue Properties of Superelastic NiTi Wires, *SMST-2000: Proceedings of the International Conference on Shape Memory and Superelastic Technologies*, S.M. Russell and A.R. Pelton, Eds., International Organization on SMST, 2001, p 397–403
9. D. Tolomeo, S. Davidson, and M. Santinoranont, Cyclic Properties of Superelastic Nitinol: Design Implications, *SMST-2000: Proceedings of the International Conference on Shape Memory and Superelastic Technologies*, S.M. Russell and A.R. Pelton, Eds., International Organization on SMST, 2001, p 471–476
10. T. Sawaguchi, G. Kaustrater, A. Yawny, M. Wagner, and G. Eggeler, Crack Initiation and Propagation in 50.9 at pct Ni-Ti Pseudoelastic Shape-Memory Wires in Bending-Rotation Fatigue, *Metall. Mater. Trans. A*, 2003, **34A**, p 2847–2860
11. "Standard Test Method for Determination of Transformation Temperature of Nickel-Titanium Shape Memory Alloys by Bend and Free Recovery," F2082-06, ASTM International, p 1–7
12. "Standard Terminology for Nickel-Titanium Shape Memory Alloys," F2005-05, ASTM International, p 1–3
13. L. Tan and W.C. Crone, In Situ TEM Observation of Two-Step Martensitic Transformation in Aged NiTi Shape Memory Alloy, *Scripta Metall. Mater.*, 2004, **50**, p 819–823
14. T.W. Duerig, Some Unsolved Aspects of Nitinol, *Mater. Sci. Eng. A-Struct.*, 2006, **438**, p 69–74
15. P.H. Adler, W. Yu, A.R. Pelton, R. Zadno, T.W. Duerig, and R. Baressi, On the Tensile and Torsional Properties of Pseudoelastic NiTi, *Scripta Metall. Mater.*, 1990, **24**, p 943–947
16. W.M. Huang and H.K. Lim, Evolution of Energy Dissipation and the Young's Modulus in a Martensite NiTi Shape Memory Alloy Wire Upon Cyclic Loading, *J. Mater. Sci. Lett.*, 2003, **22**, p 1399–1400
17. J.E. Schaffer, A Probabilistic Approach to Modeling Microstructural Variability and Fatigue Behavior in ASTM F562 Medical Grade Wire, in *Proceedings of the 9th International Congress on Fatigue, Fatigue 2006*, Atlanta, Georgia, USA, Elsevier Inc., Saint Louis, MO, USA, 2006
18. T.W. Duerig and K.N. Melton, Diffuse Yield Drop and Snap Action in a NiTi Alloy, *Materials Research Society Proceedings, Materials Research Society*, Vol. 245, 1992, p 159–167
19. A.L. McKelvey and R.O. Ritchie, Fatigue Crack Growth Behavior in the Superelastic and Shape Memory Alloy Nitinol, *Metall. Mater. Trans. A*, 2001, **32A**, p 731–743